Reversible binding and rapid diffusion of proteins in complex with inositol lipids serves to coordinate free movement with spatial information

Gerald R.V. Hammond,[1] Yirong Sim,[1] Leon Lagnado,[2] and Robin F. Irvine[1]

[1]Department of Pharmacology, University of Cambridge, Cambridge CB2 1PD, England, UK
[2]Medical Research Council Laboratory of Molecular Biology, Cambridge CB2 2QH, England, UK

Polyphosphoinositol lipids convey spatial information partly by their interactions with cellular proteins within defined domains. However, these interactions are prevented when the lipids' head groups are masked by the recruitment of cytosolic effector proteins, whereas these effectors must also have sufficient mobility to maximize functional interactions. To investigate quantitatively how these conflicting functional needs are optimized, we used different fluorescence recovery after photobleaching techniques to investigate inositol lipid–effector protein kinetics in terms of the real-time dissociation from, and diffusion within, the plasma membrane. We find that the protein–lipid complexes retain a relatively rapid (~0.1–1 $\mu m^2/s$) diffusion coefficient in the membrane, likely dominated by protein–protein interactions, but the limited time scale (seconds) of these complexes, dictated principally by lipid–protein interactions, limits their range of action to a few microns. Moreover, our data reveal that GAP1^{IP4BP}, a protein that binds PtdIns(4,5)P_2 and PtdIns(3,4,5)P_3 in vitro with similar affinity, is able to "read" PtdIns(3,4,5)P_3 signals in terms of an elongated residence time at the membrane.

Introduction

The inositol lipids regulate a wide range of cellular functions, from signal transduction to lipid transport (Balla, 2006; Di Paolo and De Camilli, 2006). As rare constituents on the cytosolic face of membranes, one of the principle means by which these lipids exert their function is through the recruitment of cytosolic proteins that contain lipid-binding motifs (Cho and Stahelin, 2005; Lemmon, 2008). Once restricted to the two-dimensional membrane surface, the increased local concentration of these proteins facilitates their interaction with binding partners and substrates.

Many interacting motifs bind specifically to a particular inositol lipid with high affinity, whereas others are more promiscuous, with a lower affinity that requires a secondary interaction for recruitment (Carlton and Cullen, 2005; Lemmon, 2008). The most abundant inositol lipid-binding motif in eukaryotic genomes is the pleckstrin homology (PH) domain (Yu et al., 2004; Lemmon, 2008). Many high-affinity PH domains bind to the D-3 phosphorylated inositol lipids phosphatidylinositol 3,4,5-trisphosphate (PtdIns(3,4,5)P_3) and phosphatidylinositol (3,4)-bisphosphate (PtdIns(3,4)P_2), whose synthesis is driven by activated cell surface receptors (Park et al., 2008); this causes recruitment of the PH domain–containing proteins to the plasma membrane, where they participate in the subsequent signal transduction cascade. However, the majority of PH domains bind with little selectivity and with lower affinity to inositol lipids (Yu et al., 2004; Lemmon, 2008). Examples include the cytohesin family of ARF guanine nucleotide exchange factors: in these, the 3G splice variants bind with low affinity and selectivity to phosphatidylinositol 4,5-bisphosphate (PtdIns(4,5)P_2) and PtdIns(3,4,5)P_3 (Klarlund et al., 2000), and their plasma membrane recruitment is assisted by an interaction with ARF-like GTPases (Cohen et al., 2007; Hofmann et al., 2007; Li et al., 2007).

Because the inositol lipids may be quite sparsely distributed on the cytosolic face of membranes, binding proteins must retain sufficient mobility to meet their interacting partners. Recent estimates place the lateral diffusion coefficients of PtdIns(4,5)P_2 and PtdIns(3,4,5)P_3 at 0.5–1 $\mu m^2/s$ (Haugh et al., 2000;

Correspondence to Gerald R.V. Hammond: gruh2@cam.ac.uk; or Robin F. Irvine: rfi20@cam.ac.uk

Abbreviations used in this paper: PH, pleckstrin homology; PLCδ1, phospholipase Cδ1; PtdIns(4,5)P_2, phosphatidylinositol 4,5-bisphosphate; PtdIns(3,4,5)P_3, phosphatidylinositol 3,4,5-trisphosphate; TIRF, total internal reflection fluorescence; SPT, single particle tracking.

The Rockefeller University Press $30.00
J. Cell Biol. Vol. 184 No. 2 297–308
www.jcb.org/cgi/doi/10.1083/jcb.200809073

Yaradanakul and Hilgemann, 2007; Golebiewska et al., 2008). Measurements in model membranes and the outer leaflet of plasma membranes yield a value threefold higher, which suggests that endogenous PtdIns(4,5)P_2 is spending two thirds of its time in complex with slow or immobile membrane components (Golebiewska et al., 2008). Furthermore, previous work has shown that several proteins maintain a comparable mobility when bound to inositol lipid as when free in the cytosol (Brough et al., 2005).

The picture is further complicated by the ability of inositol lipids to act at a more local level within a given membrane (Haugh et al., 2000). For example, localized synthesis of PtdIns(3,4,5)P_3 at the leading edge of motile cells (coupled to its degradation toward the sides and rear) is required for efficient cell motility (see Discussion for further examples; Kolsch et al., 2008). Therefore, as well as maintaining sufficient mobility to form interactions, inositol lipid effector proteins must be constrained from diffusing too far from the site of lipid synthesis, because if they do, as long as they "mask" the inositol lipid head group, they will protect it from metabolism, and so "smear out" the lipid gradient.

So, how can free mobility be reconciled with a constrained localization in the same membrane? One possibility is that an inositol lipid-bound protein retains lateral mobility but is corralled into specific membrane subdomains, such as cholesterol-enriched "rafts" (Pike and Miller, 1998) or actin-based "picket fences" (Morone et al., 2006). Alternatively, the protein may rapidly exchange between the bound and free states, which, coupled to rapid diffusion through the cytosol, leads to repeated sampling of the target membrane (Teruel and Meyer, 2000; Matsuoka et al., 2006).

In this study, we assess quantitatively the mechanisms governing spatial and temporal recruitment of PH-domain containing proteins to the membrane. Specifically, we concentrate on proteins with high-affinity PH domains, targeted to the plasma membrane via their interaction with PtdIns(4,5)P_2 and/or PtdIns(3,4,5)P_3. FRAP techniques are used that can discriminate lateral diffusion on the membrane versus exchange between bound and unbound molecules. Our results suggest that, whereas the protein–lipid complexes retain free lateral diffusion (~0.1–1 $\mu m^2/s$), they are constrained by the short-lived (seconds) time scale of this interaction.

Results

FRAP of proteins in complex with inositol lipids using total internal reflection fluorescence (TIRF)

The central aim of this paper was to distinguish lateral diffusion of inositol lipid-bound proteins from their exchange with an unbound, cytosolic pool. Therefore, we conceived a FRAP experiment whereby the entire basal membrane could be bleached selectively by TIRF microscopy, a technique that allows the imaging of the plasma membrane adherent to a glass coverslip (Axelrod, 2001). Fig. 1 A shows HEK cells expressing GFP fused to the isolated PH domain from phospholipase Cδ1 (PLCδ1) and the PH domain–containing protein GAP1^{IP4BP}, both of which are targeted to the plasma membrane by interaction with PtdIns(4,5)P_2 (Várnai and Balla, 1998; Cozier et al., 2000). Also shown (Fig. 1 A, top) is YFP targeted to the plasma membrane by the palmitoylation and myristoylation sequence from Lyn kinase (PM-YFP). Epifluorescence images of the adhesion plane, or "footprint," show the uniform haze from the basal plasma membrane, along with a ring of lateral membrane. Conversely, only uniform fluorescence in the footprint is seen

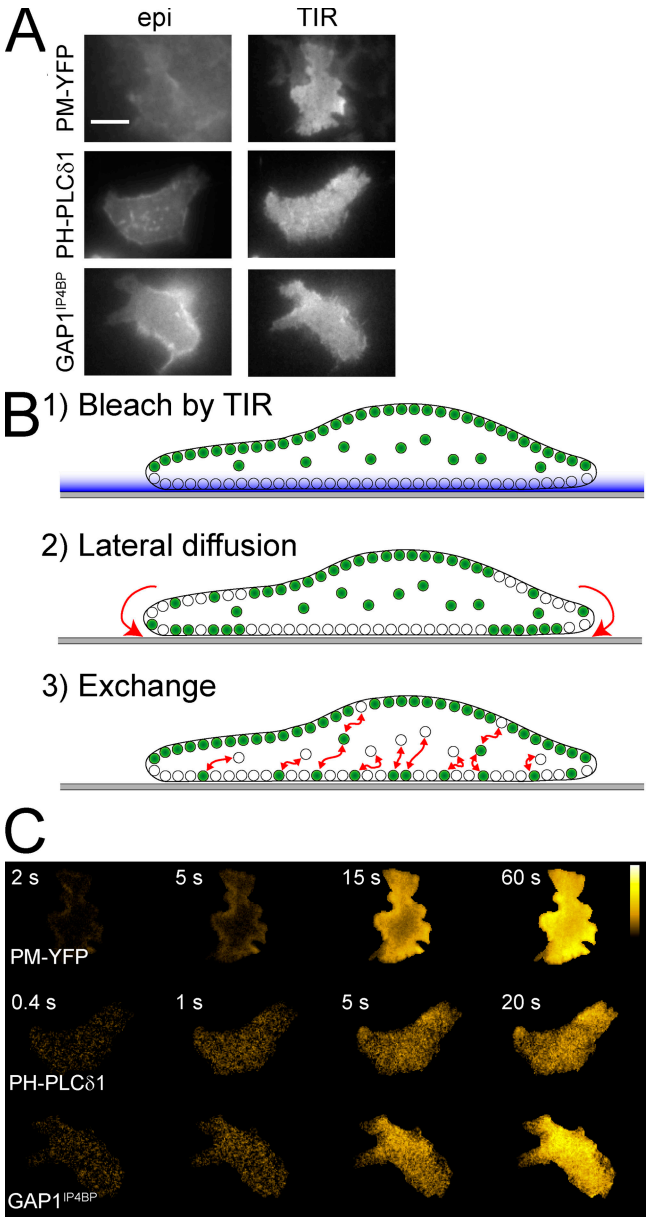

Figure 1. **FRAP by total internal reflection.** (A) Epifluorescence and TIR fluorescence micrographs of the adhesion planes ("footprints") of HEK cells expressing either the myristoylated and palmitoylated sequence of Lyn kinase fused to YFP (PM-YFP), GFP fused to the PH domain of PLCδ1, or GFP fused to full-length GAP1^{IP4BP} as indicated. The latter two are targeted to the plasma membrane via an interaction with PtdIns(4,5)P_2. (B) The rationale behind the FRAP experiment: after bleaching by TIR (1), entry of unbleached protein into the adhesion plane via lateral diffusion through the membrane should cause fluorescence recovery from the periphery (2), whereas exchange with a cytosolic pool would lead to uniform recovery across the footprint (3). (C) Example micrographs taken at the indicated times after an 8-s bleach; residual postbleach fluorescence was subtracted from the images (see Fig. S1 for details, available at http://www.jcb.org/cgi/content/full/jcb.200809073/DC1). Stills are taken from Videos 1–3. Bar, 10 μm.

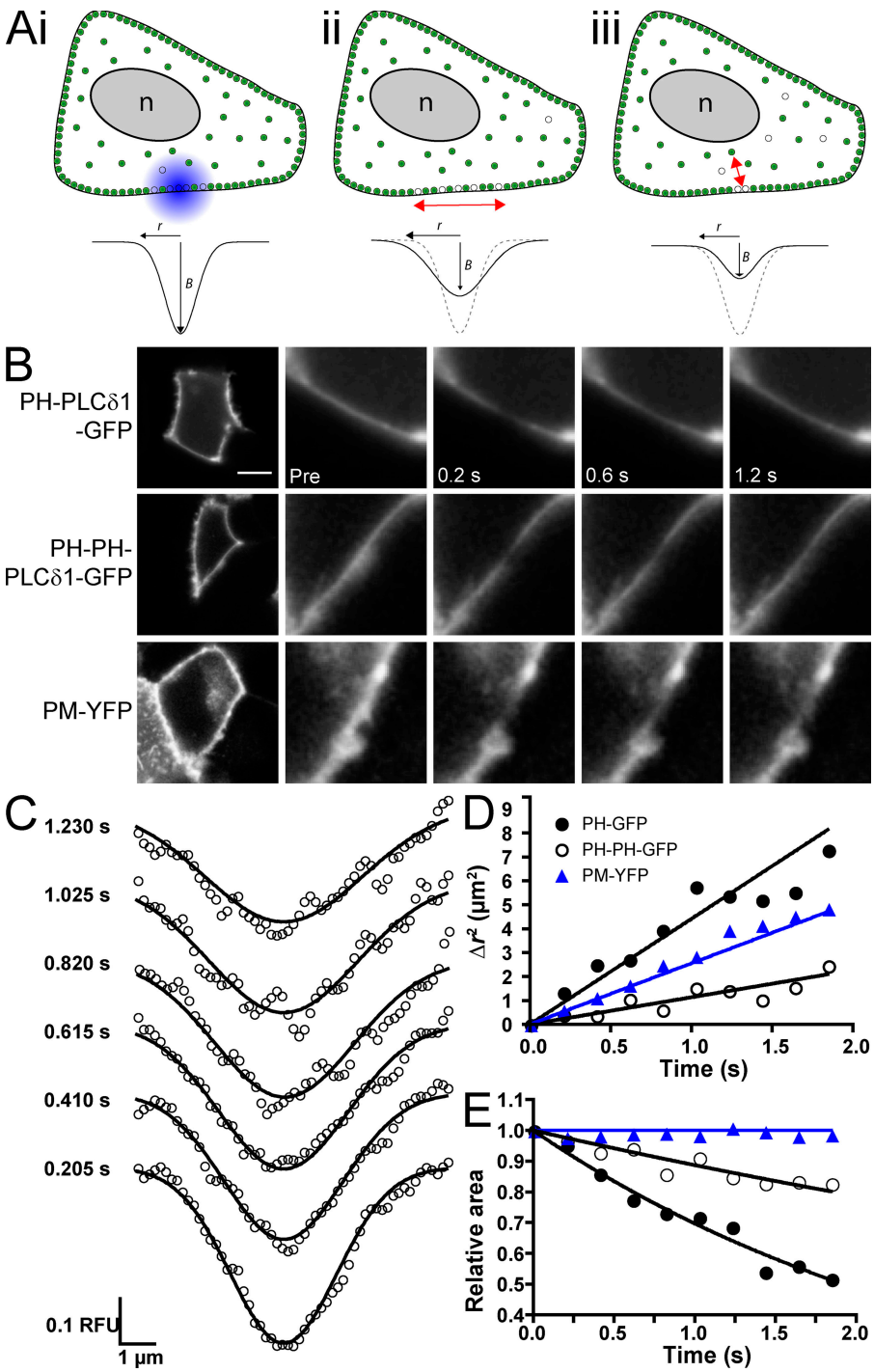

Figure 2. **Fitting diffusion coefficients and dissociation time constants to Gaussian bleach profiles.** (A) Rationale behind the experiment: illustrations show a GFP-tagged protein targeted to the plasma membrane; the membrane-bound pool of protein is assumed to be at equilibrium with a smaller, cytosolic pool. After bleaching with a pulse of light from a laser beam with a Gaussian intensity profile (i), the fluorescence intensity profile along the membrane will reflect this profile and have a defined Gaussian radius *r* and depth *B*. Lateral diffusion of bleached molecules along the plane of the membrane causes a widening of the profile radius *r*, while maintaining area under the curve (ii); conversely, exchange with the cytoplasmic pool maintains the radius but leads to a decrease in the area under the curve (iii). The model described in Eq. 2 accounts for both processes. (B) Fluorescence micrographs before bleaching of HEK cells expressing either single or tandem PH domains from PLCδ1 fused to GFP, or PM-YFP. The enlarged images show the bleached area at indicated times after bleaching. Bar, 10 µm. (C) Membrane fluorescence intensity profiles at the indicated postbleach times for the PH-GFP cell shown in B; the lines represent fits produced from Eq. 2 (see Materials and methods). (D and E) Data points show the changes in gaussian radius *r* (D) or the area under the curve (E) from membrane intensity profiles fitted with Eq. 1; the lines show the predicted diffusion coefficients *D* and membrane dissociation times τ established by fits of these curves with Eq. 1.

by TIRF when the evanescent field decays with a length constant of ∼100 nm (Fig. 1 A). Consistent with a previous paper (van Rheenen et al., 2005), we saw no local enrichment of these PtdIns(4,5)P_2-binding proteins in the adhesion plane.

We reasoned that the recovery of fluorescence in the footprint after photobleaching by TIRF would then proceed via two mechanisms: lateral diffusion through the membrane, which would approach from the border of the footprint where the basal membrane is continuous with the apical surfaces, and exchange with the overlying cytosolic pool, which would occur uniformly throughout the footprint (Fig. 1 B).

To achieve substantial photobleaching of fluorescence (≤50%) in the cellular footprint, we found it necessary to bleach for 8 s. To highlight the recovering fluorescence, residual fluorescence immediately after bleaching was subtracted from subsequent images, and the contrast was rescaled (this procedure is described in Fig. S1, available at http://www.jcb.org/cgi/content/full/jcb.200809073/DC1). Representative images from such experiments are presented in Fig. 1 C and Videos 1–3; as expected, PM-YFP (with its integral lipid anchors) recovered its fluorescence from the cell periphery, which is consistent with lateral diffusion in the plane of the membrane. The PtdIns(4,5)P_2-targeted

Table I. **Summary of results for all proteins analyzed in this study**

	Notes	Lipid bound	Localization	Ratio F_{PM}/F_{Cyt}	D	τ	Range (63%)	Range (95%)	*n*
					$\mu m^2/s$	*s*	*μm*	*μm*	
GFP	None	None	Cytoplasm	ND	31.36 ± 5.06	NA	NA	NA	13
PM-YFP	None	Integral	PM	ND	0.79 ± 0.06	$2.12 \times 10^{21} \pm 2.11 \times 10^{21}$	∞	∞	43
GFP-PH123-MyoX	None	PIP2 + PIP3	PM	1.15 ± 0.04	0.07 ± 0.02	6.96 ± 0.93	0.98	1.70	14
PH-PLCδ1-GFP	None	PIP2	PM	2.07 ± 0.12	1.24 ± 0.14	2.44 ± 0.27	2.46	4.26	52
PH-PLCδ1^{R40L}-GFP	None	None	Cytoplasm	ND	21.47 ± 3.01	NA	NA	NA	21
GFP-PH-PH-PLCδ1	None	PIP2	PM	3.49 ± 0.17	0.24 ± 0.02	11.13 ± 1.83	2.29	3.97	33
PH-PH-PLCδ1-GFP	None	PIP2	PM	4.45 ± 0.40	0.28 ± 0.03	11.08 ± 2.01	2.50	4.33	30
PH^{R40L}-PH-PLCδ1-GFP	None	PIP2	PM	2.13 ± 0.12	0.34 ± 0.05	2.87 ± 0.26	1.40	2.43	30
PH-PLCδ1-GFP	CHO-M1	PIP2	PM	1.66 ± 0.11	0.60 ± 0.10	2.21 ± 0.22	1.63	2.82	15
GFP-PH-PH-PLCδ1	CHO-M1	PIP2	PM	2.99 ± 0.27	0.05 ± 0.01	7.03 ± 0.77	0.85	1.48	13
GFP-GAP1^{m}	LY	None	Cytoplasm	ND	3.96 ± 0.66	NA	NA	NA	28
	Insulin	PIP3	PM	1.52 ± 0.08	1.33 ± 0.29	3.42 ± 0.44	3.02	5.23	30
GFP-GAP1^{IP4BP}	LY	PIP2	PM	2.55 ± 0.11	0.35 ± 0.04	3.50 ± 0.26	1.57	2.72	40
	Insulin	PIP2 + PIP3	PM	4.44 ± 0.27	0.27 ± 0.02	6.46 ± 1.12	1.86	3.22	46
GFP-GAP1^{IP4BP}	10 μM Wmn	None	Cytoplasm	ND	4.62 ± 0.54	NA	NA	NA	19
GFP-GAP1^{IP4BP}-ΔC2	LY	PIP2	PM	2.33 ± 0.13	0.41 ± 0.04	3.34 ± 0.50	1.65	2.85	36
	Insulin	PIP2 + PIP3	PM	4.28 ± 0.27	0.49 ± 0.04	7.93 ± 1.78	2.79	4.84	38
GFP-PH-GAP1^{IP4BP}	LY	PIP2	PM	3.31 ± 0.18	0.59 ± 0.04	3.64 ± 0.38	2.07	3.58	51
	Insulin	PIP2 + PIP3	PM	4.99 ± 0.37	0.70 ± 0.04	7.37 ± 1.06	3.21	5.56	47

All experiments were in HEK cells unless otherwise stated. The localization of the protein (either plasma membrane [PM] or cytoplasm) is noted, along with the lipid bound (PtdIns(4,5)P_2 or PtdIns(3,4,5)P_3). The parameters are the ratio of fluorescence at the PM verses the cytoplasm (ratio of F_{PM}/F_{Cyt}) as a crude index of membrane recruitment, lateral diffusion coefficient (*D*), and membrane dissociation time constant (τ). The range refers to the expected distance traveled on the membrane for the proportion of these proteins indicated in parentheses, and are estimated as $\sqrt{(2 \times D \times \tau)}$ for 63% and $\sqrt{(2 \times D \times 3 \times \tau)}$ for 95%, respectively (Teruel and Meyer, 2000). NA, not applicable; ND, not determined.

proteins, however, showed a uniform recovery of fluorescence across the footprint, which suggests recovery via exchange with the overlying cytosol.

Together, these experiments suggest that over the scale of a cellular footprint (~10 μm) and a time period of several seconds, exchange between bound and unbound molecules dominates recovery. However, because an extended time period was required for bleaching relative to the recovery time, we cannot determine quantitatively (a) the time course of this exchange and (b) whether there is lateral diffusion of the bound molecules.

Spot bleaching to measure lateral diffusion and membrane dissociation

To quantify lateral diffusion and membrane dissociation, we turned to a simpler bleaching paradigm (Fig. 2 A) developed by Oancea et al. (1998) to quantify lateral diffusion and dissociation of diacylglycerol-binding C1 domains. Here, a laser-scanning microscope is used, and bleaching is achieved via a brief (10 ms) pulse of light centered on the plasma membrane (Fig. 2 B). Because the laser beam has a Gaussian intensity profile, a Gaussian distribution can be fit to the bleach profile (Fig. 2 A, i), as long as the cellular fluorescence is not completely photobleached toward the center of the beam. Experiments with fixed cells confirmed these criteria, and Gaussian fits to the bleach profile showed the maximum extent of bleaching in the center of the profile to be 83 ± 1.4% ($n = 6$; unpublished data). Lateral diffusion of bleached molecules along the membrane causes a widening of this profile while conserving the area under the curve; the rate of change of the square of the Gaussian radius with time is proportional to the apparent lateral diffusion coefficient *D* (Fig. 2 A, ii; Fig. 2 D; and Materials and methods). Conversely, dissociation of bleached molecules from the membrane and their replacement with unbleached protein causes a decrease in the area of this Gaussian profile, without a change in the radius. Assuming the majority of bleached material is the protein bound to the membrane, and there is little change in the total cellular levels of unbleached protein, it has previously been shown that the dissociation rate constant governs fluorescence recovery (Bulinski et al., 2001). Thus, a membrane dissociation time constant τ can be found that should be the reciprocal of the dissociation rate constant (Fig. 2 A, iii; and Fig. 2 E; see Discussion). A simple relationship (Oancea et al., 1998) has been shown to account for simultaneous lateral diffusion *D* and dissociation τ, and can assign values to each parameter (Fig. 2 C and Materials and methods).

The bleaching and subsequent imaging were performed with the pinhole on the confocal laser scanning microscope (CLSM) fully open in order to produce an extended bleach region above and below the plane of focus. Thus, recovery of fluorescence from the z axis (which could occur by diffusion but not change the Gaussian radius) should be excluded. To test whether this assumption was correct, we used PM-YFP, which, being integral to the inner leaflet of the plasma membrane, should recover solely by lateral diffusion. As expected, this protein displayed lateral diffusion (Fig. 2 D) and usually showed no apparent displacement from the membrane (Fig. 2 E). Considering all

the cells imaged ($n = 43$), a range of dissociation time constants τ were found, from 9.6 s to $\sim 10^{22}$ s; the lower value suggests that in certain cases, diffusion from above and below the focal plane was contributing to recovery. However, the range of values collectively produces a mean value for τ that is essentially infinite (Table I), which led us to conclude that the model accurately assigns lateral diffusion verses dissociation across a sufficient sample size.

To further verify our approach, we considered a protein whose lateral diffusion coefficient had already been determined by single particle tracking (SPT), namely the three tandem PH domains from myosin X. Spot bleaching yielded an estimated D of ~ 0.07 μm^2/s (Table I), which is in excellent agreement with measurements by SPT in fibroblasts of 0.06–0.1 μm^2/s (Mashanov and Molloy, 2007). The protein also displayed an apparent τ of ~ 7 s (Table I); note that this is longer than the time for which a single protein can be tracked (because of bleaching), which is why this parameter could not be determined by SPT (Mashanov and Molloy, 2007).

This model also assumes that lateral diffusion in the cytoplasm is rapid and thus does not affect the plasma membrane profile. To test this assumption, we also determined cytoplasmic diffusion coefficients, again from spot bleaching and the subsequent rate of increase of a Gaussian radius (Fig. 3), as described in Seiffert and Oppermann (2005). Cytosolic diffusion of GFP was estimated as ~ 31 μm^2/s (Table I), which is consistent with previous estimates; e.g., Braeckmans et al. (2007) and Brough et al. (2005).

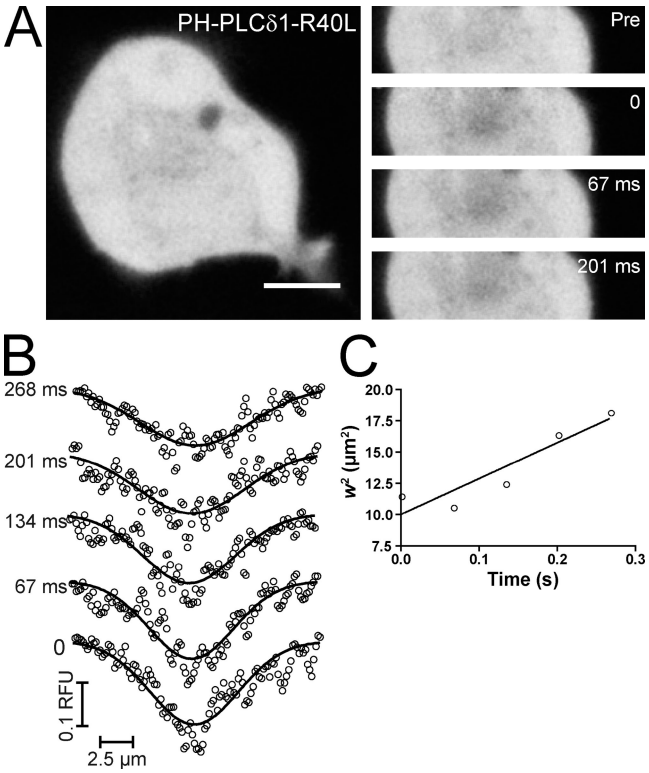

Figure 3. **Estimating cytoplasmic diffusion coefficients.** (A) A HEK cell expressing the R40L mutant of the PH-PLCδ1-GFP; the enlarged images show the strip of the cell imaged at the indicated times after bleaching. Bar, 10 μm. (B) Fluorescence intensity profiles across the bleached spot at the indicated times after bleaching; lines are fitted from the Gaussian function described in Eq. 3. (C) Increase in the square of the Gaussian width w with time is fitted in terms of the diffusion coefficient D using Eq. 4; see Materials and methods for details.

Studies of the PtdIns(4,5)P_2-binding PH domain form PLCδ1

The PH domain from PLCδ1 binds with high affinity and specificity to PtdIns(4,5)P_2 both in vitro (Garcia et al., 1995; Lemmon et al., 1995) and in cells (Várnai and Balla, 1998), where it is localized to the plasma membrane (Fig. 4 A). Lateral diffusion of this probe on the membrane was rapid, ~ 1.2 μm^2/s (Fig. 4 B and Table I; see Fig. 2 D for an example), a speed similar to that of its PtdIns(4,5)P_2 ligand (Golebiewska et al., 2008), which suggests that the lipid limits diffusion. Consistent with this, we used a point mutation of arginine 40, which renders the domain incapable of high affinity PtdIns(4,5)P_2 binding (Várnai and Balla, 1998), leading to a cytosolic localization (Fig. 4 A). The cytosolic protein is very much more mobile than the membrane-bound wild type, with a D of ~ 21 μm^2/s (Fig. 4 B and Table I; see Fig. 3 for an example).

The apparent membrane dissociation time for PH-PLCδ1 at the plasma membrane was 2.4 s (Fig. 4 C and Table I; see Fig. 2 E for an example). We reasoned that if this time constant reflects the time a typical molecule spends bound to a lipid (i.e., the inverse of the off-rate constant), then fusing two such PH domains in tandem should cause greater avidity and thus a longer τ. Fig. 4 C shows that such a tandem dimer, tagged at the N or C terminus, exhibited an apparent τ approximately fourfold longer than that of a single domain. That this reflects increased membrane affinity was further indicated by the cellular localization: whereas the single domains showed mainly membrane fluorescence with a weaker haze of unbound protein in the cytosol, the tandem dimers showed much less fluorescence in the cytoplasm (Fig. 4 A).

Unexpectedly, the tandem dimers also displayed a diffusion coefficient approximately fourfold lower than for the single domains (Fig. 4 B). We were concerned that this may indicate a more complex interpretation of our parameters. In particular, we could envisage a scenario whereby random walks of the proteins diffusing in the cytosol adjacent to the plasma membrane could lead to multiple collisions with the surface, and thus repeated incidences of lipid binding. Our membrane diffusion coefficient would thus represent cytosolic diffusion interrupted by occasional binding to relatively slow lipid molecules. Because the tandem PH domain would have to release two lipid molecules before it could undergo a period of rapid cytosolic diffusion, this would happen less often and the protein would thus appear to diffuse much slower.

We addressed this issue with two approaches. First, we rendered the first domain of a tandem dimer incapable of binding PtdIns(4,5)P_2 by mutation of arginine 40. As expected, this protein appeared similarly distributed to the single domain (Fig. 4 A) and yielded a similar τ (Fig. 4 C). Yet, its apparent diffusion coefficient was unchanged and identical to the wild-type tandem domains (Fig. 4 B and Table I). This indicates that D is not determined primarily by lipid binding, as posited in the preceding paragraph, but is rather caused by some other property of the protein, most likely transient binding to other, less-mobile

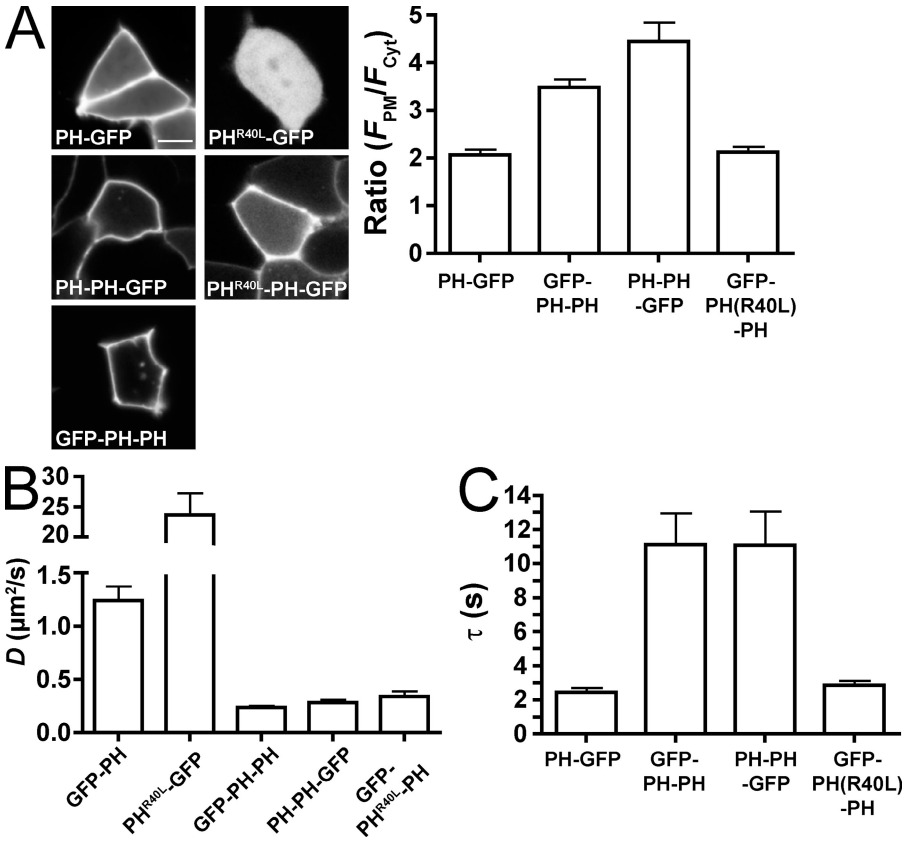

Figure 4. **Dissociation and diffusion of PH-PLCδ1.** (A) Fluorescence micrographs of HEK cells expressing single or tandem PH domains from PLCδ1 fused to GFP; where indicated, the domains carry the R40L point mutation in one of the domains. The graph on the right summarizes the ratio of fluorescence intensity at the plasma membrane relative to the cytosol for all cells analyzed, as described in Materials and methods. Bar, 10 μm. (B) Fitted diffusion coefficients; PH-GFP and PH^{R40L}-GFP are significantly different from each other and the other proteins ($P < 0.001$, Kruskall-Wallis test with a post hoc Dunn's multiple comparison test). (C) Fitted membrane dissociation time constants τ; GFP-PH-PH and PH-PH-GFP were significantly different from PH-GFP and PH^{R40L}-PH-GFP ($P < 0.001$, Kruskall-Wallis test with post hoc Dunn's multiple comparison test). Data are means ± SEM.

membrane components. If such protein–protein interactions are to regulate *D* independently of τ, they must self-evidently occur over a faster timescale than lipid–protein interactions, so again it is important to confirm that our τ calculations quantitatively reflect protein–lipid dissociation.

So, in a second approach, we estimated the membrane dissociation time via a different and completely independent method. Activation of PLC has been shown to trigger dissociation of PH-PLCδ1 from the plasma membrane in response to PtdIns(4,5)P_2 breakdown into Ins(1,4,5)P_3 and diacylglycerol (Várnai and Balla, 1998). CHO cells expressing the M1 receptor and GFP-tagged single or tandem PH domains showed rapid dissociation of membrane fluorescence in response to 1 mM carbachol (Fig. 5 A). The concomitant increase in cytosolic fluorescence could be fitted by a single exponential time constant (Fig. 5 B).

Making the assumption that PLC cannot hydrolyze PtdIns(4,5)P_2 when it is bound by a PH domain, we can envisage the following scenarios: if a PH domain makes multiple, transient interactions with the lipid while diffusing through the cytosol in the plane of the membrane, then activation of PLC will reduce the free PtdIns(4,5)P_2 levels, thus decreasing the chances of the PH domain meeting another lipid and hence accelerating its dissociation from the membrane. So, its τ by PLC activation would be shorter than that measured at steady state by spot bleaching. Alternatively, if the steady-state measurement reflects the time for a single PtdIns(4,5)P_2-PH domain complex to dissociate, this value of τ will limit how fast the protein can dissociate after activation of PLC because the enzyme will have to "wait" for the PH domain to release its bound lipid before the latter can be hydrolyzed.

We observed (a) that the value of τ in response to PLC activation or by bleaching was significantly longer for the tandem dimer than the isolated domains and that, (b) importantly, for each protein, τ was not significantly different when comparing the values derived from the two methods (Fig. 5 C). Therefore, we conclude that the membrane dissociation time τ does indeed represent the time for individual protein–lipid complexes to dissociate; i.e., it is the reciprocal of the dissociation rate constant (and so is related to affinity).

Studies of the RAS GTPase-activating proteins GAP1^m and GAP1^{IP4BP}

GAP1^m contains a PH domain with high affinity for PtdIns(3,4,5)P_3, and so translocates to the plasma membrane in response to PI 3-kinase activation (Lockyer et al., 1999). HEK cells transfected with GFP-GAP1^m and incubated in serum-free medium and a PI 3-kinase inhibitor (to ensure no production of PtdIns(3,4,5)P_3) showed cytosolic fluorescence (Fig. 6 A) and a rapid diffusion coefficient of ∼4 μm^2/s (Fig. 6 B and Table I). Conversely, addition of insulin to the cells in serum-containing medium induces PtdIns(3,4,5)P_3 synthesis and partial translocation of the protein to the plasma membrane (Fig. 6 A), where, like PH-PLCδ1, it exhibits a slower *D* of around ∼1.3 μm^2/s (Fig. 6 B) and a τ of ∼3.4 s (Table I). This confirms that when bound to membranes, GFP-GAP1^m retains a high mobility (Brough et al., 2005), though that earlier study overestimated the *D* by not taking dissociation into account, thus missing the detectable decrease in *D* value caused by membrane binding (Table I).

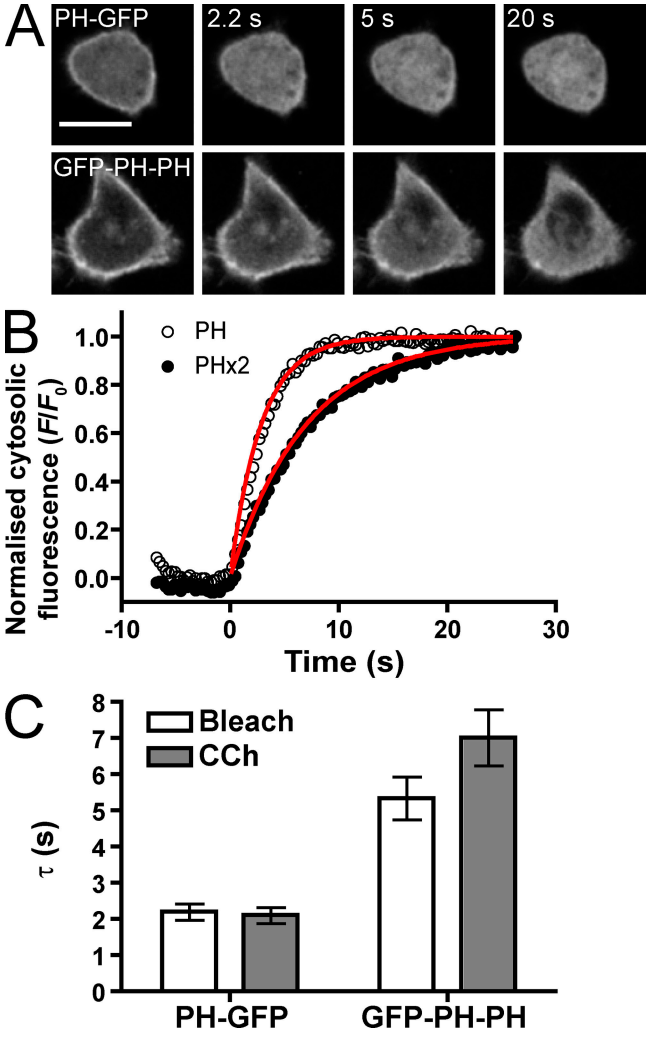

Figure 5. **Membrane dissociation of PH-PLCδ1 in response to carbachol (CCh).** (A) CHO-M1 cells expressing single or tandem PH domains either before or at the indicated times after addition of 1 mM CCh. Bar, 10 µm. (B) Normalized cytosolic fluorescence intensity for the cells shown in A; CCh was added at time 0. Data are fitted to a single exponential association (red lines). (C) Before addition of CCh, cells were subjected to a spot-bleach experiment. τ values for PH-PH-GFP are significantly greater than PH-GFP ($P < 0.0001$, Mann-Whitney test) by bleaching or after CCh addition, but were not different between methods for either PH-GFP ($P = 0.85$, paired test) or GFP-PH-PH ($P = 0.13$). Data are means ± SEM.

The highly homologous GAP1^{IP4BP} makes an interesting contrast with GAP1^{m} because in addition to binding PtdIns (3,4,5)P_3, GAP1^{IP4BP} protein also binds with high affinity to PtdIns(4,5)P_2 (Cozier et al., 2000). As a result, this protein is constitutively targeted to the plasma membrane (Fig. 7 A). Under conditions of no PtdIns(3,4,5)P_3 production, there is a slight cytosolic haze of unbound protein (Fig. 7 A), but the majority is bound to the plasma membrane, where it binds with an apparent τ of ~3.5 s and moves with a lateral diffusion coefficient somewhat slower than GAP1^{m} at ~0.3 µm^2/s (see also Brough et al., 2005). Activation of PtdIns(3,4,5)P_3 synthesis in the cells leads to a minor effect on the lateral diffusion coefficient (Fig. 7 B and Table II). However, it causes an increase in the ratio of plasma membrane to cytosolic fluorescence (Fig. 7 A), as the cytosolic haze is no longer discernable in most cells. This was

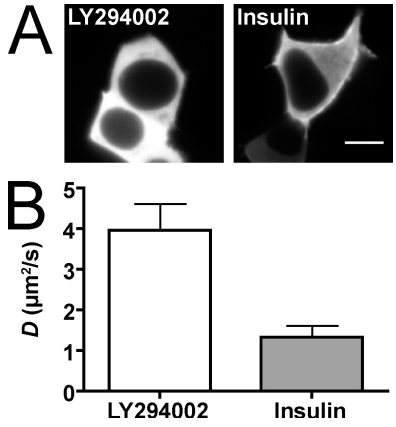

Figure 6. **Diffusion of GAP1m in the presence and absence of PtdIns (3,4,5)P_3.** (A) Fluorescence micrographs of HEK cells expressing GFP-GAP1^{m} after 1 h stimulation with 100 nM insulin in 10% serum, or 5 µM LY294002 in serum-free medium as indicated. Bar, 10 µm. (B) Diffusion coefficients under the above conditions; cytosolic diffusion in the presence of LY294002 is significantly faster than on the membrane in the presence of insulin ($P < 0.0001$, Mann-Whitney test). Data are means ± SEM.

accompanied by a nearly twofold increase in the dissociation time (Fig. 7 C). This result was unexpected because even at the height of PI 3-kinase activation, plasma membrane PtdIns (3,4,5)P_3 levels reach only a fraction (<10%) of PtdIns(4,5)P_2 levels (Stephens et al., 1993), but it does suggest that GAP1^{IP4BP} can recognize receptor-generated PtdIns(3,4,5)P_3, and this in turn points to the possibility that it might be a PtdIns(3,4,5)P_3 effector.

GAP1^{IP4BP} can be displaced from the membrane by high concentrations of wortmannin, most likely because of inhibition of PI 4-kinase activity and depletion of PtdIns(4,5)P_2 (Cozier et al., 2000). Incubation of cells with 10 µM wortmannin led to cytosolic localization of the protein, where it diffused much faster at ~4.6 µm^2/s (Table I), which is very similar to GAP1^{m} (as seen also by Brough et al., 2005).

The PH domain of GAP1^{IP4BP} was shown to be necessary for its inositol lipid-dependent targeting to the plasma membrane (Lockyer et al., 1997). To investigate if it was also sufficient to explain the protein's slower lateral mobility and dissociation compared with GAP1^{m}, we produced two truncations. First, we removed the two N-terminal C2 domains (ΔC2), as these are known to contribute to membrane targeting in other proteins (Cho and Stahelin, 2005; Lemmon, 2008). Second, we produced the isolated PH domain (Fig. 7 A). Both truncations localized

Table II. **Differences between diffusion coefficients of GAP1^{IP4BP} truncations**

	ΔC2	PH
5 µM LY294002		
Full length	NS	$P < 0.01$
ΔC2	NA	NS
100 nM insulin		
Full length	$P < 0.001$	$P < 0.001$
ΔC2	NA	$P < 0.05$

Results are from a Kruskal-Wallis test with a post hoc Dunn's multiple comparison test, and are considered significant at $P < 0.05$. NA, not applicable; NS, not significant.

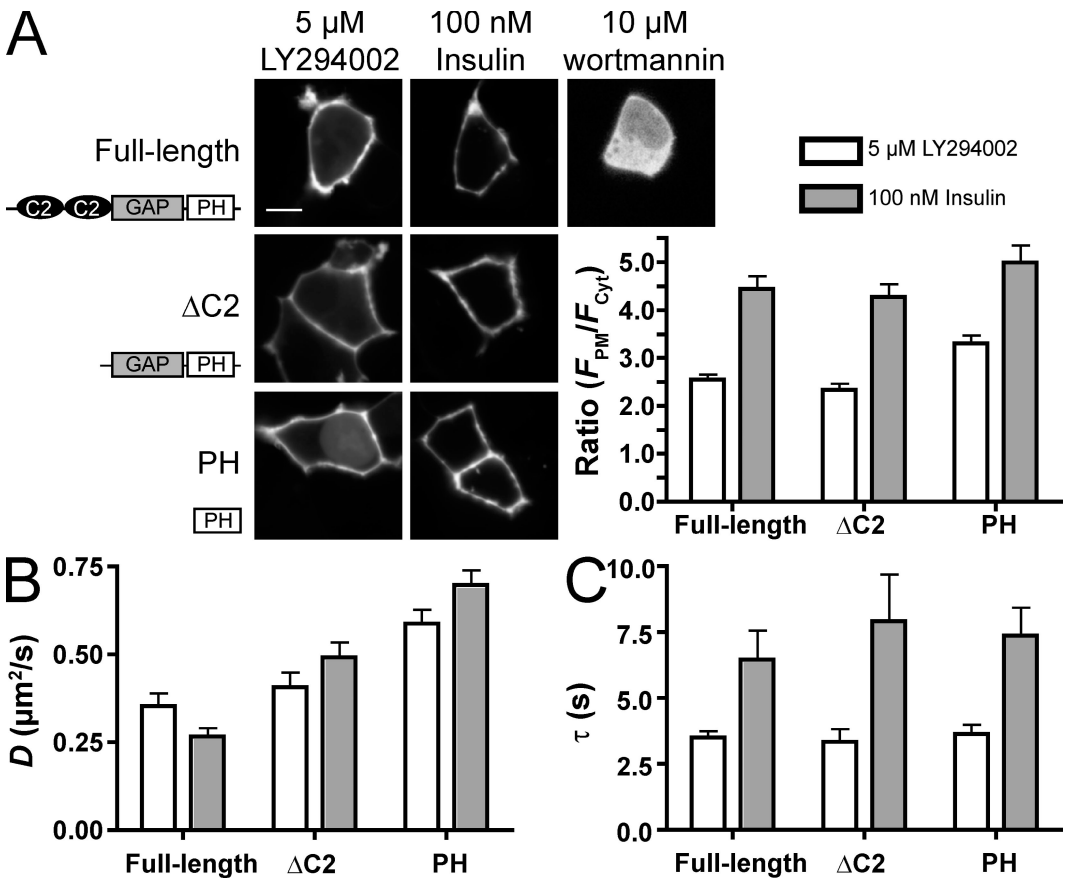

Figure 7. **Diffusion and dissociation of GAP1^{IP4BP} bound to PtdIns(4,5)P_2 ± PtdIns(3,4,5)P_3.** (A) Domain organization in the primary sequence of GAP1^{IP4BP} and its truncations. The fluorescence micrographs show HEK cells expressing the indicated constructs after 1 h stimulation with 100 nM insulin + 10% serum, 5 μM LY294002, or 10 μM wortmannin. Bar, 10 μm. (inset) The graph shows the ratio of fluorescence intensity at the plasma membrane relative to the cytosol for all cells analyzed. The fitted diffusion coefficients *D* and membrane dissociation times τ are shown in B and C, respectively. Results of statistical analysis are shown in Tables II and III. Data are means ± SEM.

identically to the full-length protein, with the exception of the PH domain, which was partially localized to the nucleus in the absence of PtdIns(3,4,5)P_3, explaining its slightly high plasma membrane–to–cytosolic fluorescence ratio (Fig. 7 A). Notably, in the presence or absence of PtdIns(3,4,5)P_3 production, τ did not differ from the full-length protein (Fig. 7 C and Table III), which confirms that the PH domain is not only sufficient for inositol lipid binding of GAP1^{IP4BP} but also dictates the kinetics of that binding.

There was little effect of PtdIns(3,4,5)P_3 generation on the lateral diffusion coefficient of the isolated PH domain of GAP1^{IP4BP} (Fig. 7 B), and it clearly showed a *D* that was approximately twofold faster than the full-length protein with or without PtdIns(3,4,5)P_3 and was also faster than the ΔC2 truncation (Fig. 7 B and Table II). Note that the difference between full-length and ΔC2 protein was less clear, as the only significant difference was in the presence of PtdIns(3,4,5)P_3 (Table II). We conclude that, as for the PH domain from PLCδ1, lipid binding to the PH domain largely dictates the membrane dissociation time. Lateral diffusion, however, is limited by interactions beyond the lipid–protein interaction, likely with other proteins, which, as discussed earlier, would be over a faster timescale than the lipid–protein interaction. Moreover, in the case of GAP1^{IP4BP}, these interactions involve parts of the protein beyond the PH domain, although we cannot reach a definitive conclusion from these data as to whether the C2 domains influence this lateral mobility.

Discussion

Our results show that the PH domain–containing proteins studied here spend seconds bound to the membrane but, during this short interaction, are able to undergo appreciable lateral diffusion of ∼1 μm²/s. Using these values, the mean distance proteins will travel on the membrane before a defined fraction dissociates can be estimated as equal to $\sqrt{(2 \times D \times \tau)}$ (Teruel and Meyer, 2000); these estimated values are also presented in Table I as "Range" of a protein before either 63% or

Table III. **GAP1^{IP4BP} and truncations treated with insulin versus LY294002**

GAP1^{IP4BP}	Ratio (F_{PM}/F_{Cyt})	D	τ
Full length	P < 0.0001	P = 0.0633	P = 0.0006
ΔC2	P < 0.0001	P = 0.2077	P < 0.0001
PH	P < 0.0001	P = 0.0373	P < 0.0001

Results are from a Mann-Whitney test. Results are considered significant at P < 0.05. No difference between full length, ΔC2, or PH was observed for the values of τ after either insulin or LY294002 treatment (Kruskal-Wallis test with a post hoc Dunn's multiple comparison test, P > 0.05).

95% dissociates. What is clear is that, despite appreciable mobility on the membrane, the inositol lipid-bound proteins studied here do not travel farther than a distance of ~1–3 µm from where they bind. This range is a little farther than that described for the *Dictyostelium discoideum* CRAC protein, which binds PtdIns(3,4,5)P_3 with an estimated τ of 0.12 s and diffuses at 0.14 µm^2/s (Matsuoka et al., 2006), giving an estimated range of ~0.2 µm.

Our estimates are consistent with the qualitative data obtained by TIR bleaching (Fig. 1). Consider a typical HEK cell with a footprint 16 µm in diameter: it might take a single molecule of PH-PLCδ1 ~40 s to diffuse from the periphery to the center of the cell, but it dissociates with a τ of ~2.4 s (Table I). Indeed, during the 8-s bleaching period, the majority of PH-PLCδ1 and GAP1^{IP4BP} molecules will have dissociated from the membrane, explaining why mobility on the scale of a cellular footprint (~10 µm) is dominated by dissociation from the membrane, as opposed to lateral diffusion.

This limited diffusion of inositol lipid-binding proteins has important functional implications. Free diffusion of the inositol lipids themselves, coupled to subcellular distributions of the enzymes that modify their head groups, can lead to the generation of local inositol lipid signals: many studies highlight the importance of PtdIns(3,4,5)P_3 generated at the leading edge of cells for efficient cell motility (Kolsch et al., 2008), and local PtdIns(3,4,5)P_3 signals are also required for epithelial cell polarity (Gassama-Diagne et al., 2006). Other examples include local generation of PtdIns(4,5)P_2 at the cleavage furrow during cytokinesis (Emoto et al., 2005; Field et al., 2005) and at regions of endocytosis and actin dynamics in adipocytes (Huang et al., 2004). Notably, all these locally produced inositol lipid signals have dimensions of micrometers. Hence, the limited diffusion of effector proteins described here (Table I) show that once recruited to these regions, the rapid diffusion of the proteins will allow them to thoroughly explore the locality of the signal and make functional interactions, whereas their dissociation ensures the lipid–effector complexes do not stray too far from the locally directed lipid synthesis. This provides a mechanism for inositol–lipid-mediated recruitment of proteins to specific regions of the plasma membrane.

The upper limit of the diffusion coefficients for the proteins described herein (Table I) are in good agreement with those described for the lipids themselves (Haugh et al., 2000; Yaradanakul and Hilgemann, 2007; Golebiewska et al., 2008) at ~1 µm^2/s; this makes sense given that the higher viscosity of the lipid bilayer produces a greater hindrance to lateral diffusion than the aqueous cytosol (Saffman and Delbrück, 1975). However, we are left with the curious observation that lateral diffusion on the membrane varies over an order of magnitude for the different proteins, irrespective of their membrane dissociation times (see Table I). Short-lived interactions or retention in membrane corrals that hinder free diffusion manifest as a slower diffusion coefficient when they occur over a much faster time scale than the measurements performed in this study (Ritchie et al., 2005). A similar suggestion has been made for PtdIns(4,5)P_2, which exhibits slower diffusion in cells than in vitro, suggesting that the major fraction is transiently bound by immobile membrane components (Golebiewska et al., 2008). SPT has shown that full-length PLCδ1 shows anomalous diffusion that is consistent with trapping in 0.7-µm membrane partitions (Mashanov and Molloy, 2007). A popular idea is that such partitions might consist of viscous, cholesterol-enriched microdomains ("rafts"). However, the inositol lipids contain polyunsaturated fatty acid tails, and so they have been shown to partition into cholesterol-enriched fractions only through electrostatic interactions between the head group and polybasic proteins such as NAP-22 (Epand et al., 2004). PH domains bind inositol lipids via a deep canonical binding pocket (Lemmon, 2008), effectively screening the head group. This would exclude head group–assisted partitioning, and so we would expect PH domain–lipid complexes to be excluded from any such localization.

The membrane dissociation times described here vary between 2 and 7 s (Table I). As discussed in the results, these times most likely reflect the dissociation rate constants (k_{off}) for the lipid–protein complexes, and are therefore a determinant of affinity between a PH domain and its ligand, given by $K_D = k_{off}/k_{on}$. This leads to interesting implications for the kinetics and affinities of PH domain–inositol lipid interactions. Dissociation constants (K_D) for high-affinity PH domain interactions of the type studied here are in the micromolar range (Garcia et al., 1995; Lemmon et al., 1995; Cozier et al., 2000); so, assuming that these estimates apply in vivo, our measured dissociation times in turn lead to k_{on} values for binding of the order of 10^5 $M^{-1}s^{-1}$, significantly slower than a diffusion-limited binding (which would be nearer to 10^7 $M^{-1}s^{-1}$; Shoup et al., 1981; Lauffenburger and Linderman, 1996). A similarly low value was estimated from in vitro binding experiments with several PH domains (Manna et al., 2007) and suggests that formation of an inositol lipid–PH domain complex follows more complex, reaction-limited kinetics. Such kinetic parameters can include accessory interactions with other anionic lipids within the membrane (Garcia et al., 1995; Corbin et al., 2004) or possible hydrophobic interactions between the bound PH domain and the membrane (Flesch et al., 2005; Manna et al., 2007). Nonetheless, an on-rate constant of 10^5 $M^{-1}s^{-1}$ predicts translocation of proteins in the nanomolar-to-micromolar concentration range to inositol lipid signals with micromolar concentration (Stephens et al., 1993) within seconds, which is consistent with experimental measurements for translocation of PH domains to newly generated inositol lipids; e.g., Haugh et al. (2000) and Várnai and Balla (1998).

Materials and methods

DNA constructs

PH-PLCδ1-GFP wild type and R40L mutant (Várnai and Balla, 1998), and the GFP- PH-PLCδ1 × 2 (van Rheenen et al., 2005) were gifts of T. Balla (National Institute of Child Health and Human Development, Bethesda MD) and K. Jalink (the Netherlands Cancer Institute, Amsterdam, Netherlands). The tandem PH-PH-GFP and PH(R40L)-PH-GFP from PLCδ1 were made by insertion of a second, wild-type domain in-frame into the respective PH-PLCδ1-GFP constructs at BamH1 sites, as described previously (van Rheenen et al., 2005). PH123-MyoX (Mashanov et al., 2004) was a gift of M. Peckham (University of Leeds, Leeds, England, UK). GFP-GAP1^{m} and GFP-GAP1^{IP4BP} were as described previously (Lockyer et al., 1997). The isolated PH domain of GAP1^{IP4BP} was amplified from the full-length construct via PCR using the primers 5′-CGGAATTCTGTGCTTAAAGAAGGGTTC-3′ (forward) and 5′-TGCTCGCCCTGCACTGGCTAAGGTACCCC-3′

(reverse), and cloned into pEGFP-C1 (Clontech Laboratories, Inc.) at EcoR1–BamH1 sites (underlined). The ΔC2 domain truncation was amplified using 5′-GCGAGCTCGCCTAAAGCCAGACGACC-3′ (forward) and 5′-CCTCCACTCATTCCATTTAAGGTACCGG-3′ (reverse), and cloned into pEGFP-C1 at Sac1–Kpn1 sites (underlined). PM-YFP is the palmitoylated/myristoylated N-terminal 11 residues of human Lyn kinase (MGCIKSKGKDS) cloned into pEYFP-N1 (Clontech Laboratories, Inc.) at EcoR1–BamH1 sites, and was a gift of T. Meyer (Stanford University, Stanford, CA). Isolated GFP was expressed from the pEGFP-N1 vector (Clontech Laboratories, Inc.). All constructs were subject to dideoxy sequencing.

Cell culture and transfection

CHO cells expressing the M1 receptor (CHO-M1) were a gift from M. Edwardson (University of Cambridge, Cambridge, England, UK). CHO-M1 and HEK 293 cells were maintained in DME supplemented with 10% FCS, 100 µg/ml penicillin, 100 units/ml streptomycin. 1 d before transfection, 50,000–100,000 cells were seeded in the central 12-mm glass-bottomed well of a 35-mm dish (WillCo Wells), which had been coated with poly-L-lysine. Cells were transfected with 2 µg DNA using 6 µg Lipofectamine 2000 (Invitrogen) in Opti-MEM (Invitrogen) according to the manufacturer's instructions. After 24 h, cells were rinsed and then imaged in DME without phenol red (Invitrogen) containing 25 mM Hepes, and supplemented with 10% FCS. 100 nM insulin (Sigma-Aldrich) was included where indicated, and the cells were preincubated for 1 h at 37°C before imaging. When cells were treated with 5 µM LY294002 (Sigma-Aldrich), 10% FCS was omitted and cells were preincubated for 1 h at 37°C before imaging.

TIRF microscopy

A custom-built "through-the-lens" TIRF microscope was used as described previously (Holt et al., 2004); essentially, this consisted of a modified inverted microscope (Axiovert S100TV; Carl Zeiss, Inc.) fitted with a 60× plan apochromatic 1.45 NA oil immersion objective (Olympus). Images were acquired at ∼5 frames/s on a Pentamax cooled charge-coupled device camera (Princeton Instruments) controlled by IPlab software (version 3.9; BD). Excitation was with the 488-nm line of an Argon ion laser (100 mW, Melles Griot), power was set to 80%, and the beam was attenuated by 99% via a neutral density filter. Photobleaching within the evanescent field was achieved by removal of the neutral density filter for 8 s. 20 frames were acquired before bleaching, and postbleach images were acquired until fluorescence recovery was complete. Experiments were performed at room temperature.

Image stacks were exported from the IPlab software as TIFF files. These were opened with ImageJ (version 1.38; http://rsb.info.nih.gov/ij/) and converted to 8 bit. The "image calculator" function was used to subtract the first postbleach image intensity from the other images in the stack to highlight the fluorescence recovery. Contrast was then adjusted to show only the first 100 gray levels (see Fig. S1).

Spot bleaching experiments

Experiments were conducted on a laser scanning confocal microscope (SP5 TCS; Leica) attached to a DMI6000 inverted microscope equipped with a 63× plan-apochromatic 1.4 NA oil immersion objective (Leica). The microscope was fitted with an environmental chamber (Solent Scientific) that maintained a steady temperature of 37°C throughout the experiments. The pinhole was opened fully (optical section, ∼1 µm) to permit maximum light acquisition, and to defocus the bleaching light beam and effectively bleach fluors above and below the focal plane. FRAP experiments were performed using the FRAP wizard within the LAS AF software= (version 1.8.2; Leica). In brief, images were scanned in bidirectional scanning mode using a line average of 2 (to reduce noise) at the maximum scan speed (1400 Hz), using either the 488-nm or 514-nm laser lines of an Argon laser for GFP and YFP, respectively. For membrane proteins, images of 256 × 256 pixels were acquired, giving ∼5 frames/s. For cytosolic proteins, a strip across the center of the cell of 256 × 16–67 pixels was imaged in order to increase the frame rate to up to 50 frames/s without line averaging. 10 prebleach frames were acquired at attenuated laser power (typically 3–5%) before bleaching with 100% laser power in a focused spot, either on the membrane or centered in the cytosol, for 10 ms. Fluorescence recovery was then followed until recovery was complete. Emitted light was collected between 500 and 550 nm (GFP), or 525 and 575 nm (YFP). Transmitted light (bright field or differential interference contrast) images were scanned in parallel to verify that cells were healthy and adherent.

To estimate the ratio of fluorescence at the plasma membrane relative to the cytosol, mean pixel intensity in a small rectangular region of interest centered on the plasma membrane was divided by the same size rectangle placed over the cytosol, as described previously (Teruel and Meyer, 2000).

Estimating the diffusion coefficient and dissociation times of membrane-bound proteins

We have used the approach defined by Oancea et al. (1998); for a discussion of the principle behind this technique, see Results.

Image stacks from spot bleach experiments in the Leica image file (lif) format were imported into ImageJ using the LOCI bioformats importer (http://www.loci.wisc.edu/ome/formats.html). Stacks were subject to 3 × 3 smoothing, and the 10 prebleach frames were averaged to form a prebleach baseline, to which all subsequent frames were normalized. Next, the segmented line tool was used to trace a line along the plasma membrane across the bleached spot; the fluorescence intensity profile along this line was then recorded for several postbleach frames in the normalized image stack, using the built-in "record profile" macro. These data were then copied into an Excel spreadsheet (Microsoft) and normalized to the total cellular fluorescence (relative to the first frame) at each time point to correct for photobleaching during acquisition.

Corrected intensity profiles were then copied into Prism 4 (GraphPad Software) and fit independently with the following Gaussian function:

$$F(x) = 1 - B \times e^{-\frac{(x-c)^2}{r^2}} \quad (1),$$

where F is the normalized fluorescence intensity, c represents the center of the bleach profile (of distance x, in µm), B represents the depth of the Gaussian profile, and r represents the Gaussian radius at e^{-1}. Fits to these three parameters from the first time point were then used to define B_0, r_0, and c for the following function (Oancea et al., 1998):

$$F(x,t) = 1 - B_0 \times \left(\frac{r_0}{\sqrt{4Dt + r_0^2}} \right) \times e^{-\frac{(x-c)^2}{\left(4Dt + r_0^2\right)}} \times e^{-\frac{t}{\tau}} \quad (2),$$

where D is the apparent lateral diffusion coefficient (in µm^2/s) and τ is the apparent membrane dissociation time (in seconds). Thus, this Gaussian function finds a single value of D and τ for the change in shape of all the profiles with time caused by lateral diffusion and membrane dissociation, respectively.

A semi-independent check was then performed for the fitted values from Eq. 2. First, the values of r^2 were calculated from those values fitted from Eq. 1; these were plotted against time, and a line on the graph was defined in terms of the value of D obtained from Eq. 2 using:

$$r^2 = 4Dt + r_0^2.$$

Second, the relative area under the curves was estimated as $\sqrt{(2\pi)}Br$, normalized to the first postbleach frame, and plotted against time. Again, a curve was plotted using Eq. 2's fitted value of τ: relative area = $e^{-(t/\tau)}$. This allowed the goodness of fit for the defined curves from Eq. 2 to be inspected, relative to the independent values of r and B fitted using Eq. 1.

Estimating the cytosolic diffusion coefficient of soluble proteins

This technique estimates the diffusion coefficient from the rate of expansion of a Gaussian bleach profile with time, as described by Seiffert and Oppermann (2005). Image stacks were normalized as described earlier for membrane proteins, and a straight line through the bleach spot was recorded from several time points. These profiles were bleach-corrected as for membrane proteins, and fit in Prism 4 using the following Gaussian function:

$$F(x) = 1 - B \times e^{-\frac{(x-c)^2}{2w^2}} \quad (3),$$

where F is the normalized fluorescence intensity, B is the depth of bleaching at the center of the spot c, and w is the full width at half maximum of the Gaussian profile. Fitted values of w^2 were then plotted against their respective time t, and the diffusion coefficient fit from:

$$w^2 = 2Dt + w_0^2 \quad (4).$$

Online supplemental material

Fig. S1 provides an outline of the normalization process used to present data from TIRF experiments. Videos 1–3 show real-time videos of the cells presented in Fig. 1 C after such normalization. Online supplemental material is available at http://www.jcb.org/cgi/content/full/jcb.200809073/DC1.

We are most grateful to our colleagues (listed in Materials and methods) who generously sent us DNA constructs. We also thank Stuart MacLaughlin for many helpful insights, and Justin Molloy, Claire Cheetham, and members of the Irvine laboratory for useful discussions.

Y. Sim was supported by the Cambridge MB/PhD program. This work was supported by a Program Grant from the Wellcome Trust.

Submitted: 10 September 2008
Accepted: 18 December 2008

References

Axelrod, D. 2001. Total internal reflection fluorescence microscopy in cell biology. *Traffic.* 2:764–774.

Balla, T. 2006. Phosphoinositide-derived messengers in endocrine signaling. *J. Endocrinol.* 188:135–153.

Braeckmans, K., K. Remaut, R.E. Vandenbroucke, B. Lucas, S.C. De Smedt, and J. Demeester. 2007. Line FRAP with the confocal laser scanning microscope for diffusion measurements in small regions of 3-D samples. *Biophys. J.* 92:2172–2183.

Brough, D., F. Bhatti, and R.F. Irvine. 2005. Mobility of proteins associated with the plasma membrane by interaction with inositol lipids. *J. Cell Sci.* 118:3019–3025.

Bulinski, J.C., D.J. Odde, B.J. Howell, T.D. Salmon, and C.M. Waterman-Storer. 2001. Rapid dynamics of the microtubule binding of ensconsin in vivo. *J. Cell Sci.* 114:3885–3897.

Carlton, J.G., and P.J. Cullen. 2005. Coincidence detection in phosphoinositide signaling. *Trends Cell Biol.* 15:540–547.

Cho, W., and R.V. Stahelin. 2005. Membrane-protein interactions in cell signaling and membrane trafficking. *Annu. Rev. Biophys. Biomol. Struct.* 34:119–151.

Cohen, L.A., A. Honda, P. Varnai, F.D. Brown, T. Balla, and J.G. Donaldson. 2007. Active Arf6 recruits ARNO/cytohesin GEFs to the PM by binding their PH domains. *Mol. Biol. Cell.* 18:2244–2253.

Corbin, J.A., R.A. Dirkx, and J.J. Falke. 2004. GRP1 pleckstrin homology domain: activation parameters and novel search mechanism for rare target lipid. *Biochemistry.* 43:16161–16173.

Cozier, G.E., P.J. Lockyer, J.S. Reynolds, S. Kupzig, J.R. Bottomley, T.H. Millard, G. Banting, and P.J. Cullen. 2000. GAP1IP4BP contains a novel group I pleckstrin homology domain that directs constitutive plasma membrane association. *J. Biol. Chem.* 275:28261–28268.

Di Paolo, G., and P. De Camilli. 2006. Phosphoinositides in cell regulation and membrane dynamics. *Nature.* 443:651–657.

Emoto, K., H. Inadome, Y. Kanaho, S. Narumiya, and M. Umeda. 2005. Local change in phospholipid composition at the cleavage furrow is essential for completion of cytokinesis. *J. Biol. Chem.* 280:37901–37907.

Epand, R.M., P. Vuong, C.M. Yip, S. Maekawa, and R.F. Epand. 2004. Cholesterol-dependent partitioning of PtdIns(4,5)P2 into membrane domains by the N-terminal fragment of NAP-22 (neuronal axonal myristoylated membrane protein of 22 kDa). *Biochem. J.* 379:527–532.

Field, S.J., N. Madson, M.L. Kerr, K.A. Galbraith, C.E. Kennedy, M. Tahiliani, A. Wilkins, and L.C. Cantley. 2005. PtdIns(4,5)P2 functions at the cleavage furrow during cytokinesis. *Curr. Biol.* 15:1407–1412.

Flesch, F.M., J.W. Yu, M.A. Lemmon, and K.N. Burger. 2005. Membrane activity of the phospholipase C-delta1 pleckstrin homology (PH) domain. *Biochem. J.* 389:435–441.

Garcia, P., R. Gupta, S. Shah, A.J. Morris, S.A. Rudge, S. Scarlata, V. Petrova, S. McLaughlin, and M.J. Rebecchi. 1995. The pleckstrin homology domain of phospholipase C-delta 1 binds with high affinity to phosphatidylinositol 4,5-bisphosphate in bilayer membranes. *Biochemistry.* 34:16228–16234.

Gassama-Diagne, A., W. Yu, M. ter Beest, F. Martin-Belmonte, A. Kierbel, J. Engel, and K. Mostov. 2006. Phosphatidylinositol-3,4,5-trisphosphate regulates the formation of the basolateral plasma membrane in epithelial cells. *Nat. Cell Biol.* 8:963–970.

Golebiewska, U., M. Nyako, W. Woturski, I. Zaitseva, and S. McLaughlin. 2008. Diffusion coefficient of fluorescent phosphatidylinositol 4,5-bisphosphate in the plasma membrane of cells. *Mol. Biol. Cell.* 19:1663–1669.

Haugh, J.M., F. Codazzi, M. Teruel, and T. Meyer. 2000. Spatial sensing in fibroblasts mediated by 3′ phosphoinositides. *J. Cell Biol.* 151:1269–1280.

Hofmann, I., A. Thompson, C.M. Sanderson, and S. Munro. 2007. The Arl4 family of small G proteins can recruit the cytohesin Arf6 exchange factors to the plasma membrane. *Curr. Biol.* 17:711–716.

Holt, M., A. Cooke, A. Neef, and L. Lagnado. 2004. High mobility of vesicles supports continuous exocytosis at a ribbon synapse. *Curr. Biol.* 14:173–183.

Huang, S., L. Lifshitz, V. Patki-Kamath, R. Tuft, K. Fogarty, and M.P. Czech. 2004. Phosphatidylinositol-4,5-bisphosphate-rich plasma membrane patches organize active zones of endocytosis and ruffling in cultured adipocytes. *Mol. Cell. Biol.* 24:9102–9123.

Klarlund, J.K., W. Tsiaras, J.J. Holik, A. Chawla, and M.P. Czech. 2000. Distinct polyphosphoinositide binding selectivities for pleckstrin homology domains of GRP1-like proteins based on diglycine versus triglycine motifs. *J. Biol. Chem.* 275:32816–32821.

Kolsch, V., P. Charest, and R. Firtel. 2008. The regulation of cell motility and chemotaxis by phospholipid signaling. *J. Cell Sci.* 121:551–559.

Lauffenburger, D.A., and J.J. Linderman. 1996. Receptors: Models for Binding, Trafficking, and Signaling. Oxford University Press, Oxford. 376 pp.

Lemmon, M.A. 2008. Membrane recognition by phospholipid-binding domains. *Nat. Rev. Mol. Cell Biol.* 9:99–111.

Lemmon, M.A., K.M. Ferguson, R. O'Brien, P.B. Sigler, and J. Schlessinger. 1995. Specific and high-affinity binding of inositol phosphates to an isolated pleckstrin homology domain. *Proc. Natl. Acad. Sci. USA.* 92:10472–10476.

Li, C.C., T.C. Chiang, T.S. Wu, G. Pacheco-Rodriguez, J. Moss, and F.J. Lee. 2007. ARL4D recruits cytohesin-2/ARNO to modulate actin remodeling. *Mol. Biol. Cell.* 18:4420–4437.

Lockyer, P.J., J.R. Bottomley, J.S. Reynolds, T.J. McNulty, K. Venkateswarlu, B.V. Potter, C.E. Dempsey, and P.J. Cullen. 1997. Distinct subcellular localisations of the putative inositol 1,3,4,5-tetrakisphosphate receptors GAP1IP4BP and GAP1m result from the GAP1IP4BP PH domain directing plasma membrane targeting. *Curr. Biol.* 7:1007–1010.

Lockyer, P.J., S. Wennström, S. Kupzig, K. Venkateswarlu, J. Downward, and P.J. Cullen. 1999. Identification of the ras GTPase-activating protein GAP1(m) as a phosphatidylinositol-3,4,5-trisphosphate-binding protein in vivo. *Curr. Biol.* 9:265–268.

Manna, D., A. Albanese, W.S. Park, and W. Cho. 2007. Mechanistic basis of differential cellular responses of phosphatidylinositol 3,4-bisphosphate- and phosphatidylinositol 3,4,5-trisphosphate-binding pleckstrin homology domains. *J. Biol. Chem.* 282:32093–32105.

Mashanov, G.I., and J.E. Molloy. 2007. Automatic detection of single fluorophores in live cells. *Biophys. J.* 92:2199–2211.

Mashanov, G.I., D. Tacon, M. Peckham, and J.E. Molloy. 2004. The spatial and temporal dynamics of pleckstrin homology domain binding at the plasma membrane measured by imaging single molecules in live mouse myoblasts. *J. Biol. Chem.* 279:15274–15280.

Matsuoka, S., M. Iijima, T.M. Watanabe, H. Kuwayama, T. Yanagida, P.N. Devreotes, and M. Ueda. 2006. Single-molecule analysis of chemoattractant-stimulated membrane recruitment of a PH-domain-containing protein. *J. Cell Sci.* 119:1071–1079.

Morone, N., T. Fujiwara, K. Murase, R.S. Kasai, H. Ike, S. Yuasa, J. Usukura, and A. Kusumi. 2006. Three-dimensional reconstruction of the membrane skeleton at the plasma membrane interface by electron tomography. *J. Cell Biol.* 174:851–862.

Oancea, E., M.N. Teruel, A.F. Quest, and T. Meyer. 1998. Green fluorescent protein (GFP)-tagged cysteine-rich domains from protein kinase C as fluorescent indicators for diacylglycerol signaling in living cells. *J. Cell Biol.* 140:485–498.

Park, W.S., W. Doheo, J. Whalen, N. Orourke, H. Bryan, T. Meyer, and M. Teruel. 2008. Comprehensive identification of PIP3-regulated PH domains from *C. elegans* to *H. sapiens* by model prediction and live imaging. *Mol. Cell.* 30:381–392.

Pike, L.J., and J.M. Miller. 1998. Cholesterol depletion delocalizes phosphatidylinositol bisphosphate and inhibits hormone-stimulated phosphatidylinositol turnover. *J. Biol. Chem.* 273:22298–22304.

Ritchie, K., X.Y. Shan, J. Kondo, K. Iwasawa, T. Fujiwara, and A. Kusumi. 2005. Detection of non-Brownian diffusion in the cell membrane in single molecule tracking. *Biophys. J.* 88:2266–2277.

Saffman, P.G., and M. Delbrück. 1975. Brownian motion in biological membranes. *Proc. Natl. Acad. Sci. USA.* 72:3111–3113.

Seiffert, S., and W. Oppermann. 2005. Systematic evaluation of FRAP experiments performed in a confocal laser scanning microscope. *J. Microsc.* 220:20–30.

Shoup, D., G. Lipari, and A. Szabo. 1981. Diffusion-controlled bimolecular reaction rates. The effect of rotational diffusion and orientation constraints. *Biophys. J.* 36:697–714.

Stephens, L.R., T.R. Jackson, and P.T. Hawkins. 1993. Agonist-stimulated synthesis of phosphatidylinositol(3,4,5)-trisphosphate: a new intracellular signalling system? *Biochim. Biophys. Acta.* 1179:27–75.

Teruel, M.N., and T. Meyer. 2000. Translocation and reversible localization of signaling proteins: a dynamic future for signal transduction. *Cell.* 103:181–184.

van Rheenen, J., E.M. Achame, H. Janssen, J. Calafat, and K. Jalink. 2005. PIP2 signaling in lipid domains: a critical re-evaluation. *EMBO J.* 24:1664–1673.

Várnai, P., and T. Balla. 1998. Visualization of phosphoinositides that bind pleckstrin homology domains: calcium- and agonist-induced dynamic changes and relationship to myo-[^{3}H]inositol-labeled phosphoinositide pools. *J. Cell Biol.* 143:501–510.

Yaradanakul, A., and D.W. Hilgemann. 2007. Unrestricted diffusion of exogenous and endogenous PIP(2)in baby hamster kidney and Chinese hamster ovary cell plasmalemma. *J. Membr. Biol.* 220:53–67.

Yu, J.W., J.M. Mendrola, A. Audhya, S. Singh, D. Keleti, D.B. DeWald, D. Murray, S.D. Emr, and M.A. Lemmon. 2004. Genome-wide analysis of membrane targeting by S. cerevisiae pleckstrin homology domains. *Mol. Cell.* 13:677–688.